# Implementation of a New Bank Erosion Model in Delft3D

Parsapour-Moghaddam, Parna; Rennie, Colin David; Slaney, Jonathan; Platzek, Frank; Shirkhani, Hamidreza; Jamieson, Elizabeth; Mosselman, Erik; Measures, Richard

**DOI**
10.1061/JHEND8.HYENG-13206

**Publication date**
2023

**Document Version**
Final published version

**Published in**
Journal of Hydrologic Engineering

**Citation (APA)**
Parsapour-Moghaddam, P., Rennie, C. D., Slaney, J., Platzek, F., Shirkhani, H., Jamieson, E., Mosselman, E., & Measures, R. (2023). Implementation of a New Bank Erosion Model in Delft3D. *Journal of Hydrologic Engineering*, *149*(10), Article 13206. https://doi.org/10.1061/JHEND8.HYENG-13206

# Implementation of a New Bank Erosion Model in Delft3D

Parna Parsapour-Moghaddam[1]; Colin David Rennie, M.ASCE[2]; Jonathan Slaney[3]; Frank Platzek[4]; Hamidreza Shirkhani, M.ASCE[5]; Elizabeth Jamieson[6]; Erik Mosselman[7]; and Richard Measures[8]



**Abstract:** Bank erosion plays an important role in the hydro-morphodynamics and evolution of natural rivers. Therefore, it is essential to have a reliable bank erosion model for accurate simulation of hydro-morphodynamic processes. We developed and successfully implemented a new, feasible bank erosion model in Delft3D software. The developed model considers physical bank erosion processes to a greater extent than previous models. Model performance was assessed by comparison with a previously reported experiment in a mobile-bed-and-bank laboratory open-channel bend flume. The results from our developed model were compared with those from the standard Delft3D and angle of repose bank erosion models. We showed that progressive lateral bank erosion as well as the corresponding hydro-morphodynamics of the channel were better predicted by the developed bank erosion model. The results of this study provide insight into bank erosion prediction with Delft3D, and they suggest that the developed model will improve the performance of the Delft3D model for short- and long-term hydro-morphodynamic simulation of natural meandering rivers. **DOI: 10.1061/JHEND8.HYENG-13206.** 

**Author keywords:** Delft3D model; Bank erosion; Angle of repose; Hydro-morphodynamics; Meandering rivers.

## Introduction

The morphodynamic evolution of natural streams is driven by several hydrodynamic and sediment transport processes. Bank erosion is one of these crucial processes and has significant implications for the evolution of meanders, the reshaping of banks, bank retreat, fish habitat and the river ecosystem, sediment loading, and water quality (Eaton et al. 2004; Nardi et al. 2013; Hagemann et al. 2018; Parsapour-Moghaddam et al. 2019; Rinaldi and Darby 2007; Midgley et al. 2012). Bank erosion results from the interaction of bank basal erosion and mass failure (Osman and Thorne 1988; Mosselman 1998; Duan and Julien 2005; Rinaldi and Darby 2007). Basal erosion includes lateral erosion and bed degradation due to flow-induced forces, while mass failure corresponds to the failure of unstable slopes at the bank (Darby et al. 2002; Rinaldi et al. 2008).

Numerical models have been widely used to simulate river hydrodynamics (Shimizu et al. 1990; Olsen and Stokseth 1995; Sinha et al. 2012; Parsapour-Moghaddam and Rennie 2017, 2018; Yan et al. 2020; Bulat et al. 2019) and morphodynamic processes (Khosronejad et al. 2007; Kasvi et al. 2015; Parsapour-Moghaddam et al. 2019; Theol et al. 2020; Olsen 2021). In order to have a proper understanding of river hydro-morphodynamics for river management and restoration, it is important to appropriately simulate bank erosion processes. Modeling of bank erosion processes has been implemented with various approaches. The resulting models range from simple ones that empirically estimate the bank retreat rate based on hydrodynamic parameters (Wallick et al. 2006; Larsen et al. 2006; Constantine et al. 2009; Klösch et al. 2010) to complex mechanistic models that take into account fluvial erosion, mass failure, and seepage stability (Chen and Duan 2006; Rinaldi and Darby 2007; Rinaldi et al. 2008; Abderrezzak et al. 2016; Rousseau et al. 2017).

Meander evolution models that link the migration rate of meanders to flow conditions and channel and bank material characteristics are well studied (Wallick et al. 2006; Larsen et al. 2006; Constantine et al. 2009; Klösch et al. 2010). These models mainly depend on calibration based on historical planform changes. Mechanistic bank erosion models have been developed by other scholars for particular types of bank materials or failure mechanisms (Nagata et al. 2000; Darby et al. 2002). Chen and Duan (2006) proposed an analytical model for width adjustment of meandering rivers due to both basal erosion and bank collapse processes. They simplified the bank-collapse process for noncohesive

[1]Formerly, Postdoctoral Fellow, Dept. of Civil Engineering, Univ. of Ottawa, Ottawa, ON, Canada K1N 6N5 (corresponding author). Email: pparsapo@uottawa.ca

[2]Professor, Dept. of Civil Engineering, Univ. of Ottawa, Ottawa, ON, Canada K1N 6N5. Email: colin.rennie@uottawa.ca

[3]Planning Engineer and Program Manager, Planning Engineering in the River Engineering Group, City of Calgary, P.O. Box 2100, Stn. M, Calgary, AB, Canada T2P 2M5. Email: Jonathan.Slaney@calgary.ca

[4]Software Developer, Deltares, Boussinesqweg 1, Delft 2629 HV, Netherlands. ORCID: https://orcid.org/0000-0003-3700-7794. Email: Frank.Platzek@deltares.nl

[5]Research Officer, National Research Council of Canada, 1200 Montreal Rd., Ottawa, ON, Canada K1A 0R6; Dept. of Civil Engineering, Univ. of Ottawa, Ottawa, ON, Canada K1N 6N5. Email: Hamidreza.Shirkhani@nrc-cnrc.gc.ca

[6]Senior Engineer, National Hydrological Service, Water Survey of Canada, Environment and Climate Change Canada, Gatineau, QC, Canada K1A 0H3. ORCID: https://orcid.org/0000-0003-0358-2926. Email: Elizabeth.Jamieson@ec.gc.ca

[7]Lecturer, Faculty of Civil Engineering and Geosciences, Delft Univ. of Technology, Delft CN 2628, Netherlands; Specialist and Expert Advisor, Deltares, Boussinesqweg 1, Delft HV 2629, Netherlands. ORCID: https://orcid.org/0000-0002-4335-5085. Email: Erik.Mosselman@deltares.nl

[8]Hydrodynamics Scientist, National Institute of Water & Atmospheric Research Ltd. (NIWA), P.O. Box 8602, 10 Kyle St., Riccarton, Christchurch 8011, New Zealand. ORCID: https://orcid.org/0000-0002-9746-886X. Email: Richard.measures@niwa.co.nz

Note. This manuscript was submitted on January 10, 2022; approved on May 17, 2023; published online on July 24, 2023. Discussion period open until December 24, 2023; separate discussions must be submitted for individual papers. This paper is part of the ***Journal of Hydraulic Engineering***, © ASCE, ISSN 0733-9429.

materials and showed that the rate of bankline retreat is determined by lateral erosion rate, near-bank bed degradation rate, sediment grain size, and the difference between flow depth and bank height.

Stecca et al. (2017) analyzed the performance of various bank erosion methods that could be applied in a fixed-mesh two-dimensional hydro-morphodynamics model. They tested the bank erosion methods using a one-dimensional (1D) reduced cross-sectional hydrodynamic model under the assumption of longitudinal morphodynamic equilibrium. Others have studied bank erosion modules to be used in 2D depth-integrated models for the simulation of meandering processes (Piégay et al. 2005; Duan and Julien 2005; Parker et al. 2011; Asahi et al. 2013; Harijanto 2018). Abderrezzak et al. (2016) presented a simple bank-erosion module for a 2D finite-element morphodynamic model. The numerical model of the bank-erosion is based on tilting the elements whose slope is steeper than the angle of repose of the bank material in order to bring the elements slope to the angle of repose. The model was examined via a cross section simulation of a flume experiment with uniform bank material as well as a physical model with groynes-induced bank failure. Other models have taken into account complex erosion and mass failure processes and their interactions. Rousseau et al. (2017) studied the capability of a geotechnical model coupled with a Telemac-Mascaret model (Hervouet 2007) to predict bank retreat in meandering rivers. Langendoen et al. (2016) combined TELEMAC-2D and SISYPHE (Villaret et al. 2013) models of the Telemac-Mascaret river morphodynamics suite with bank erosion modules based on the conservational channel evolution and pollutant transport system (CONCEPTS) computer model (Langendoen and Simon 2008). Lai et al. (2015) developed a river morphodynamic model by combining the sediment and river hydraulics–2D (SRH-2D) computer model (Lai 2010) with the bank stability and toe erosion model (BSTEM), which is physics-based (Simon et al. 2011). Some of the previously developed models are based on a moving-boundary–fitted coordinate system to simulate the bankline shifting caused by bank erosion (Mosselman 1998; Nagata et al. 2000; Darby et al. 2002).

Most of the widely used hydro-morphodynamic models employ simplified bank erosion modules, and remain fairly limited in simulation of the physical processes involved in bank erosion (Rinaldi et al. 2008; Langendoen et al. 2016; Williams et al. 2016; Stecca et al. 2017). Delft3D-Flow is one of the most widely used hydrodynamic models for river flow simulation (Williams et al. 2013; Kasvi et al. 2015; Javernick et al. 2016). To simulate lateral bank erosion the current version of Delft3D employs a simple scheme that transfers an erosion flux from the near-bank wet cell to the adjacent dry-bank cells (Van der Wegen et al. 2008; Deltares 2020). Rinaldi et al. (2008) made one of the first attempts to couple the Delft3D hydrodynamic model to a comprehensive riverbank dynamic model considering pore water and hydrostatic confining pressures. However, the results were limited to the particular sedimentary and morphological conditions of the study area and therefore cannot be widely employed. In addition, such an approach is computationally expensive.

Spruyt et al. (2011) and Jagers et al. (2011) proposed a new approach based on a local immersed-boundary technique for shifting banklines as separate moving objects on a fixed grid. They implemented their method in the existing framework of Delft3D. Using the open-source hydrodynamic model Delft3D as a framework, Canestrelli et al. (2016) proposed a hybrid cut-cell and ghost-cell method for continuity and momentum equations. Williams et al. (2016) used Delft3D to set up a depth-averaged model to predict the morphodynamics of a braided river reach. They conducted analyses to assess the sensitivity of the model to different factors, including two bank erosion modules; Standard Delft3D and angle of repose. Previous attempts to implement bank erosion models in Delft3D were limited in terms of generality, efficient computational cost, feasibility of integration in Delft3D source code, and consideration of long-term river morphodynamics of an entire channel. Another limitation of past efforts in bank erosion development was that performance was assessed using a reduced cross-sectional model. In this way, the complex interaction between bank failure and sediment transport may not have been considered.

We developed, implemented, and tested an improved bank erosion module in Delft3D. Our bank erosion algorithm follows one of the bank erosion models tested in Stecca et al. (2017). To evaluate its performance we compared the outcomes of the model with the results of experimental work by Jamieson et al. (2013). Our developed model was applied to the entire experimental channel to consider the interaction between the mass failure and hydro-morphodynamics of the whole channel. We show that the developed model better predicts outer bank erosion than does the Standard Delft3D model and a model based solely on the angle of repose. In the following section, we elaborate on our experimental study based on which the numerical model was developed and evaluated. We explain the methodology employed in this research and follow with results and outcomes, which we then discuss and draw conclusions from.

## Model Assessment: Data and Case Study

In order to examine the capability of the implemented bank erosion methods, we subject different bank erosion models, including the proposed model, to experimental testing. Jamieson et al. (2013) conducted laboratory flume experiments in a 135° sand-bed-and-bank channel bend in order to study flow field dynamics and bank erosion in the presence of stream barbs. They employed acoustic Doppler velocimeters (ADVs) to collect spatially dense high-frequency velocity data when the bed conditions had static bathymetry (equilibrium). Bed elevation was measured using a laser altimeter.

As shown in Fig. 1, the flume was 1.0 m wide and had a centerline length of 18.5 m, with a 12.19-m long approach section followed by a 135° bend section, with a constant radius of curvature of 1.5 m (at the channel centerline) and a straight 2.44-m long exit section. Within the 1-m wide flume, an initial trapezoidal sand channel was set with a bottom width of 0.26 m, a top width of 0.80 m, a center depth 0.148 m, and a bank angle ($\theta$) of 29° [Fig. 1(a)]. The outer bank floodplain had a width of 0.15 m. The bed material was sand with a median ($d_{50}$) diameter of 1.1 mm and with 98% of particles between 0.6 and 1.8 mm. The initial bed slope was set at 0.0007 and the flow rate was 0.021 $m^3/s$ for the bankfull flow conditions.

Experiments were performed with clear-water scour conditions where flow in the approach section was near the threshold of particle motion; negligible movement of sand grains was observed. Therefore, Jamieson et al. (2013) attributed the erosion and sedimentation in the bend to flow dynamics within the bend alone. They considered a base case run without barbs on the bank (defined as Run TR3), which represented erosion and sedimentation processes due to flow hydrodynamics and bank characteristics. Flow in Run TR3 remained at bankfull without overbank flow, but the outer bank floodplain eroded laterally until an equilibrium condition was achieved. The flume-averaged velocity ($Q/A$) and corresponding Froude number in the approach section were 0.267 m/s and 0.21, respectively. We used the TR3 run to evaluate the performance of the bank erosion models.

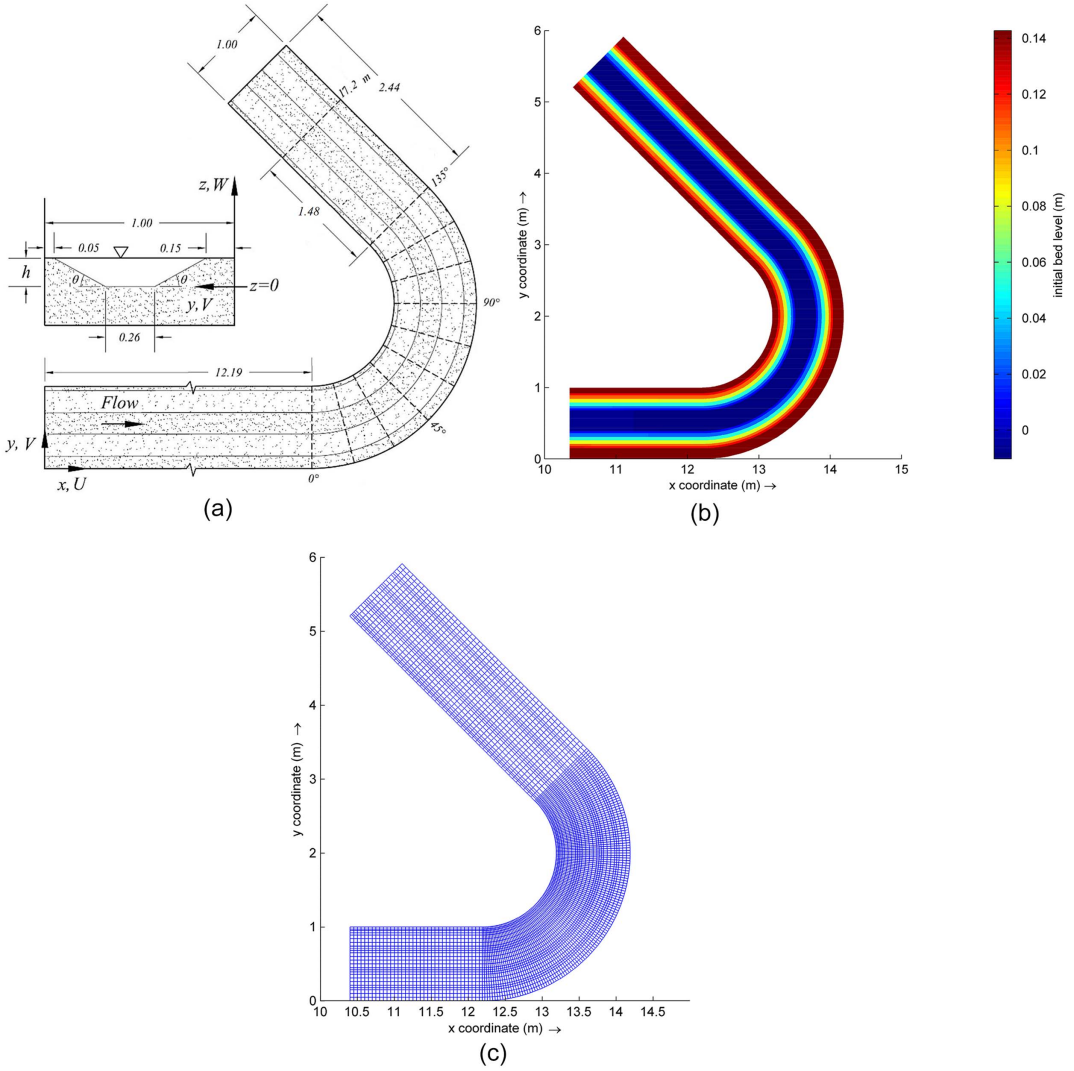


**Fig. 1.** (a) Plan and bankfull flow cross-sectional views (looking downstream) of channel (adapted from Jamieson et al. 2013); (b) bed topography data; and (c) mesh grids developed in Delft3D. Dashed lines in (a) marking 90° and 135° in the bend and 17.2 m (1.48 m downstream of the bend exit) are used for further analysis in Fig. 5.

## Methodology

### *Bank Erosion Models*

Bank erosion is a result of the combination of fluvial erosion due to flowing water and mass failure by gravity due to bank instabilities. Here we introduce a method that represents these processes through a combination of physics-based and empirical algorithms, which are not computationally expensive and are implemented relatively straightforwardly in the existing Delft3D code. In the developed model, we employed a scheme presented in Stecca et al. (2017) in which the bank erosion algorithm is broken down into two major steps: (1) slope estimation to identify the bank; and (2) estimation of bank erosion fluxes. Bank erosion models employ different approaches to identify the bank and to estimate the bank erosion flux. Next we discuss the three bank erosion models that we used in this study.

#### Standard Delft3D

In the Delft3D standard bank erosion model (Van der Wegen et al. 2008; Deltares 2020), only dry points adjacent to wet cells can be considered for bank erosion. That is, no bank slope condition is considered. The bank erosion model redistributes the erosion volume in the wet cell to the adjacent dry cells. This is determined by a user-defined percentage parameter (ThetSD) that distributes the specified percentage of the erosion in the wet cell to the adjacent dry cells. Once the dry cell gets wet, the standard bank erosion model may not work effectively since the local bed shear stresses can be too low to initiate particle motion due to fluvial erosion. Thus, the process stops and there is no more lateral erosion. This shows that there is no consideration of actual bed erosion processes such as fluvial erosion and mass failure in the estimation of the bank erosion. Hereafter, we refer to this method as the standard model.

#### Angle of Repose

Williams et al. (2016) proposed a repose scheme for bank erosion simulation and implemented the scheme in the Delft3D model. The repose scheme considers a slope failure process to occur when the bank slope exceeds a specified repose angle. The slope is calculated at cell boundaries, and when it exceeds the specified angle of repose, the bed material is transported to the toe cell toward the downslope direction. The bank slope after mass failure is assumed to reach the repose angle, and the flux of lateral bank erosion

depends only on slope exceedance from the angle of repose. The slope at cell boundaries may vary again due to the longitudinal bedload transport. Hereafter, we refer to this method as the angle of repose model.

**Developed**

Following Stecca et al. (2017), we developed a new bank erosion model to be implemented in the Delft3D code. Stecca et al. (2017) tested different bank erosion algorithms with a 1D cross-sectional model. Here we developed a model to be implemented in the source code of Delft3D. For the bank identification step, we estimated the slope at cell boundaries. Since Delft3D uses curvilinear grids, we estimated different slopes along different directions for each cell to ensure that the grid cell orientation would not restrict bank identification. Fig. 2 is a schematic of morphological grid cells in Delft3D and the directions along which the slopes are estimated. The slope for each cell, which is considered for bank erosion (the top), is measured with respect to each of the neighboring cells (the toe) in both $m$ and $n$ directions

$$S_m = \frac{(z_{\text{top}} - z_{\text{toe}})}{\Delta m} \tag{1}$$

$$S_n = \frac{(z_{\text{top}} - z_{\text{toe}})}{\Delta n} \tag{2}$$

where $z$ = bed level; and $\Delta m$ and $\Delta n$ = grid size in the $m$ and $n$ directions, respectively. The net slope is calculated as follows:

$$S_{\text{net}} = \sqrt{S_m^2 + S_n^2} \tag{3}$$

The lateral erosion of the bank is considered for the cells along the $m$ and $n$ directions for which the estimated net slope exceeds the user-defined angle of repose: $S_{\text{net}} > S_{\text{repose}}$.

As described in Stecca et al. (2017), we estimate the bank erosion rate at the top cell ($q_{\text{bank}}$) as proportional to the longitudinal bedload transport rate of the toe cell ($q_{\text{toe}}$):

$$q_{\text{bank}} = \alpha q_{\text{toe}} \tag{4}$$

where $\alpha$ = dimensionless coefficient. The range of $\alpha$ is defined to be $0 < \alpha \leq 0.1$, assuming that the sediment flux due to bank erosion is around 10 times smaller than the fluvial transport flux (Nicholas 2013; Stecca et al. 2017). The bedload transport rate at the toe ($q_{\text{toe}}$) is the bedload obtained from the total bedload transport formula applied at the toe cell. Delft3D offers a number of standard sediment transport formulations for noncohesive sediment (Deltares 2020). Eq. (4), for the $x$ and $y$ directions can be written as

$$(q_{\text{bank}})_x = \alpha (q_{\text{toe}})_y \tag{5}$$

$$(q_{\text{bank}})_y = \alpha (q_{\text{toe}})_x \tag{6}$$

The estimated bank erosion fluxes are then considered for updating the bed level at the bank and the toe cells.

It should be noted that, contrary to the angle of repose scheme, this approach estimates the flux of lateral bank erosion as a function of bank erosion at the toe cell and not just based on slope exceedance from the critical slope. This helps to have a more generic bank erosion model that is based on sediment transport processes in the entire reach rather than a specific cross section.

A major limitation of the standard bank erosion module of Delft3D is that only dry cells adjacent to wet cells are considered for bank erosion; once they get wet, lateral erosion is impeded. However, in the developed method all cells, including the wet cells on the bank, can be considered for bank erosion, given that their slopes are above the user-defined threshold.

The hydro-morphodynamic and bedload transport model employed in this study is discussed in following sections.

### Development of the Delft3D Models

We built three Delft3D models using the three aforementioned bank erosion modules: (1) standard Delft3D, (2) angle of repose, and (3) developed. Our developed model was successfully developed, implemented, and compiled in the source code of Delft3D. It should be noted that the standard bank erosion model is the default built-in feature of Delft3D. Williams et al. (2016) developed the

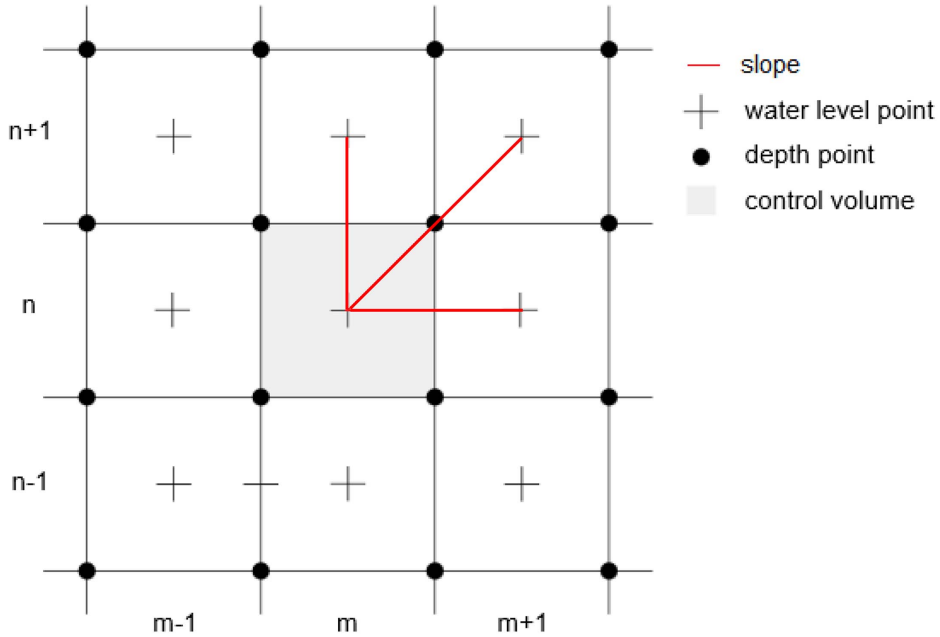


**Fig. 2.** Morphological grids and control volume. Slopes are estimated in various directions.

angle of repose model in Delft3D; we developed and implemented the developed model in Delft3D as well. We applied these models to the experimental case study to evaluate the performance of each bank erosion module. All three bank erosion models were carefully calibrated individually. The calibration parameters in the bank erosion module included the ThetSD parameter (ThetSD = 1) for the standard Delft3D model and the angle of repose slope equivalent parameter ($S_{repose} = 0.35$) for both the developed and the angle of repose models. The dimensionless $\alpha$ in the proposed bank erosion module was also considered a calibration parameter ($\alpha = 0.1$), calibrated based on sensitivity analysis within the range of values suggested in the literature (Nicholas 2013; Stecca et al. 2017). Through an iterative process, we minimized the differences between channel bed elevations obtained by the developed model and those from the experimental test.

In the following sections, we describe the hydrodynamic and morphodynamic models used identically for three models. The hydrodynamic model was calibrated (roughness and background horizontal eddy viscosity) using the standard Delft3D bank erosion module, and then applied with the same hydrodynamic parameter values in the calibration of the other two modules.

### Hydrodynamic Model

We considered 3D hydrodynamic modeling of the experimental domain using the Delft3D modeling package (Delft3D-FLOW version 4.01.01). Delft3D is a freely available open-source code developed by Deltares that employs a rectilinear or a curvilinear grid for hydrodynamic modeling. The Delft3D hydrodynamic model solves the 3D Navier-Stokes equations for incompressible flow. We assumed the shallow-water condition where the vertical momentum equation is reduced to the hydrostatic pressure assumption. We applied Reynolds averaging to the 3D Navier-Stokes equations. Delft3D employs various turbulence closure models to solve the Reynolds Averaged Navier-Stokes (RANS) equations. The Delft3D-Flow code applies a mixed finite-difference/finite-volume method. In the vertical direction, we employed a $\sigma$-coordinate system in which five vertical layers were bounded by the planes that follow the free surface and the bottom topography. The average cell area in the horizontal direction was $2 \times 10^{-3}$ m$^2$ with finer grid cells near the banks. For more details on 3D hydrodynamic modeling, readers are referred to Deltares (2020).

The initial bed topography [Fig. 1(b)] was developed to replicate the initial bed levels in the flume with the same slope as the flume (0.0007). As Fig. 1(c) shows, the horizontal grids were generated based on an orthogonal curvilinear grid covering the model domain. The average grid size in the cross-stream direction was 4 cm with the finest grid size of 1 cm near the banks along the entire channel. The grid size in the streamwise direction varied along the channel. The mesh had $430 \times 26$ cells, with average cell areas in the approach channel, the bend section, and the downstream straight section of 20, 10, and 30 cm$^2$, respectively. In the vertical direction, five layers were used regardless of depth ($\sigma$-coordinate) with nonuniform distribution of the layers in the depth. Layer thicknesses were equivalent to 2%, 8%, 20%, 30%, and 40% of the depth. A mesh-independence analysis was conducted to ensure that the hydrodynamic model was mesh resolution–independent. The mesh was further refined to ensure that there were no significant changes in the hydrodynamic results. The mean absolute difference and mean absolute relative difference were used to measure the changes in velocity and water level obtained from the two meshes. Because the velocity near the banks might be very small, even a small change could result in significant relative differences. Therefore, the centerline of the channel was used for velocity comparison while the water levels were compared on all grid cells. The results of the mesh-independence tests for the three meshes are presented in Table 1, where each row represents the results of the mesh-independence test compared with the results of the coarser mesh. The mesh with $430 \times 26$ cells was selected since, for both water level and velocity, the mean relative differences relative to the finer mesh ($430 \times 33$ cells) were not significant (<1%).

The developed grids were also examined to ensure mesh quality in terms of aspect ratio (<2) and orthogonality (deviations < 0.05). The 3D $k$-$\varepsilon$ turbulence model was used to consider 3D turbulent mixing. The hydrodynamic model was calibrated using Manning roughness ($n = 0.011$) and background horizontal eddy viscosity ($\nu = 0.01$ m$^2$/s). A flume discharge of 21 L/s was applied at the upstream boundary of the domain, and the downstream water level was set as the bankfull flow condition like that in the experimental setup. Bed shear stress was estimated based on the flow velocity just above the bed.

### Morphodynamic Model

The study flume contained noncohesive (sand) bed materials. The morphodynamic Delft3D model is capable of simulating the bedload for noncohesive sediments using a number of standard noncohesive sediment transport formulations. We assumed a homogeneous sediment with one sediment fraction ($d_{50} = 1.1$ mm) for the sediment transport estimation. Sediment transport in the experimental work was governed by the bedload transport induced by the streamwise and transverse secondary flows. In order to simulate the bedload transport, we employed Van Rijn equations. They provided the bedload rate magnitude and direction. The bedload transport rate is estimated as

$$q_b = 0.006 \rho_s w_s d_{50} M^{0.5} M_e^{0.7} \tag{7}$$

where $\rho_s$ = sediment density; $w_s$ = fall velocity; $M$ = sediment mobility number; and $M_e$ = excess sediment mobility number. The sediment mobility and excess sediment mobility numbers are defined as

$$M = \frac{v_{eff}^2}{(s-1) g d_{50}} \tag{8}$$

**Table 1.** Statistics of velocity comparison for mesh-independence test

| No. of cells in mesh | Velocity | | Water level | |
|---|---|---|---|---|
| | Mean relative absolute difference (%) | Mean absolute difference (m/s) | Mean relative absolute difference (%) | Mean absolute difference (m) |
| $430 \times 15$ | — | — | — | — |
| $430 \times 26$ | 1.3 | $3.9 \times 10^{-3}$ | 0.35 | $6.1 \times 10^{-3}$ |
| $430 \times 33$ | 0.8 | $2.7 \times 10^{-3}$ | 0.11 | $5.3 \times 10^{-3}$ |

$$M_e = \frac{(v_{eff} - v_{cr})^2}{(s-1)gd_{50}} \tag{9}$$

where $v_{cr}$ = critical depth-averaged velocity for initiation of motion based on the Shields curve; and $v_{eff}$ = magnitude of an equivalent depth-averaged velocity based on the logarithmic velocity profile assumption computed in the bottom computational layer. The projection of the sediment transport intensity is computed in the direction of the near-bed flow.

In order to account for the transverse bed slope effect, an additional bedload transport vector is calculated perpendicular to the main bedload transport

$$q_b' = \beta\sqrt{\tau_{cr}/\tau_b}S_T q_b \tag{10}$$

where $\tau_{cr}$ and $\tau_b$ = critical and near-bed shear stress, respectively; $S_T$ = bed slope in the direction normal to the bedload transport vector; and $\beta$ = user-defined coefficient set to 1.5. The computed bedload transport due to the transverse bed slope is then added to the bedload transport estimated in Eq. (7).

## Results

In this section, we evaluate the performance of the three bank erosion models: (1) standard, (2) angle of repose, and (3) developed. In addition to the first two models, which were already embedded in Delft3D, we implemented our proposed model in the Delft3D source code. We developed 3D hydro-morphodynamic models that employ the three bank erosion models to simulate the abovementioned experimental work.

To ensure that the hydrodynamic model was calibrated appropriately, predicted bed shear stress was compared with observed bed shear stress . The local shear velocity ($U_*$) and the bed shear stress ($\tau_0 = \rho U_*^2$) in the primary channel approach section were estimated from the vertical profile of velocity near the center of the 11.5-m cross section, which was sufficiently downstream of the flume entrance to ensure that the flow was fully developed while ensuring that there was no bend influence upstream of the bend. The shear velocity and bed shear stress during the experiment were 0.156 m/s and 0.244 N/m$^2$; those obtained from the model were 0.158 m/s and 0.250 N/m$^2$.

Due to the complex nonlinear interactions between hydrodynamic and morphological processes, bank erosion processes can affect hydrodynamic and fluvial transport in the entire reach. Therefore, to assess the performance of the standard, angle of repose, and developed bank erosion models, we applied them to the entire reach rather than a single cross section. After reaching bathymetric equilibrium, we compared the simulated bed level changes and velocity fields with the results of the experimental work in Jamieson et al. (2013). The capabilities of the bank erosion models were evaluated on their ability to simulate the bank erosion observed in the experimental work as well as the velocity field induced by changes in the bed level.

Fig. 3 shows the simulated cumulative erosion and deposition for the experimental work as well as all three numerical models. The results from the experimental study [Fig. 3(a)] show scour along the outer bank with maximum erosion occurring downstream of the bend exit at Cross section 135° [see Fig. 1(a)]. Due to transportation of the eroded material from the outer bank toward the inner bank, deposition occurred in the center of the channel, particularly downstream of the bend exit. As Fig. 3(b) shows, the developed model reproduced the extent of the bank erosion in the outer bank and the maximum erosion downstream of the bend exit. Moreover, although less than that observed in the experiment, our model predicted deposition in the center of the channel. The standard Delft3D bank erosion model did not erode the full width of the outer bank floodplain; it was not able to reproduce the bank erosion in the outer bank because the lateral erosion stopped as soon as the dry cell became wet [Fig. 3(c)]. The angle of repose model did simulate bank erosion at the outer bank downstream of the bend exit [Fig. 3(d)], but it caused considerable erosion at the inner bank and upstream of the bend as well as corresponding deposition in the center of the channel toward the inner bend, none of which were observed during the experimental study. This unrealistic prediction of the erosion at both the inner bank and upstream of the bend could be attributed to the angle of repose algorithm, where the slope exceedance resulted in bank erosion regardless of the hydrodynamic and morphodynamic conditions.

Fig. 4 shows the differences in bed level obtained by all three models with respect to the measured bed level, and Table 2 shows the mean absolute error (MAE) and the root-mean-square error (RMSE) of the bed level simulation obtained from each model relative to the experimental results. In addition, Table 2 provides the bias of the differences between model results and measurements for both erosion and deposition. Our developed model had the least difference overall and well predicted the outer bank erosion, particularly downstream of the bend exit—the location of maximum erosion (difference $\approx 0$). On the other hand, the standard Delft3D model did not predict the bank erosion along the outer bank. Both models underestimated the deposition in the center of the channel. Finally, the angle of repose model had the largest overall bed elevation differences, particularly along the inner bank.

Fig. 5 shows in detail the resulting bed level from the three models at Cross sections 90°, 135°, and 1.48 m downstream of the bend exit [section locations are shown in Fig. 1(a)]. The downstream section was selected as it was the location of greatest overall scour, so it best represented the ability of each model to predict recession of the outer bank. The maximum observed erosion and deposition depths in the 90°-, 135°-, and 1.48-m cross sections are provided in Table 3 and compared with those obtained from the models. As can be seen, the results indicate satisfactory performance for our developed model. It should be noted that prediction of the magnitude of maximum erosion and deposition in the cross section was not sufficient to assess model performance; the location of the observed erosion and deposition was of essential importance. For instance, as Figs. 3 and 4 show, the developed model outperformed the other models in predicting the maximum erosion along the outer bank, which is critical for an appropriate bank erosion simulation.

As Fig. 5 shows, although the standard bank erosion model well predicted the thalweg elevation at the downstream section, it did not permit near-bank erosion in the outer bank. Therefore, instead of lateral erosion, the model caused a steep scour hole along the outer bank side slope. The angle of repose model induced erosion in both banks throughout the bend. Deposition of this additionally recruited sediment resulted in better prediction of the observed mid-channel deposition in the bend, but ultimately resulted in excess recession of both banks. On the other hand, by the downstream section the developed model best predicted the erosion pattern at the outer bank and reasonably predicted the bed level changes throughout the section observed during the experiment. Overall, the results in Figs. 3–5 and Table 2 show that the Delft3D model with our developed module outperformed the other methods. In addition, the results indicate that it is essential to evaluate the performance of bank erosion models when they are applied to the entire channel.

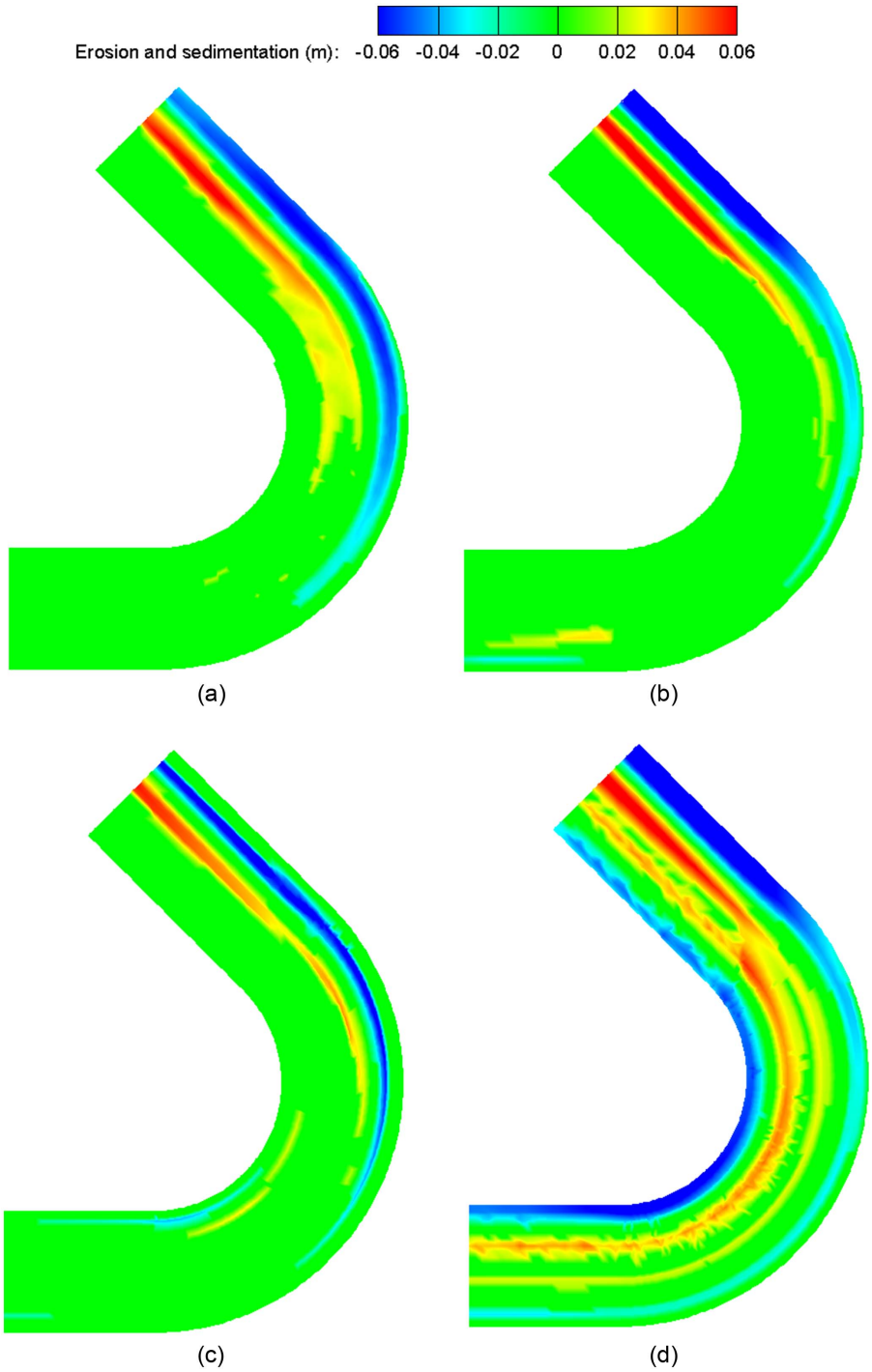


**Fig. 3.** Bed level changes obtained from (a) experimental work; (b) developed bank erosion model; (c) standard Delft3D model; and (d) angle of repose model. Negative and positive values indicate erosion and deposition, respectively.

Hydrodynamic and morphodynamic river processes are strongly coupled. That is, any change in river morphodynamics results in changes in river hydrodynamics and vice versa. We investigated the effect of bank erosion processes on streamwise and cross-stream velocities in the channel against experimental observations. The velocity magnitude and the secondary velocities are presented for two cross sections in the channel: 90° and 135° in Figs. 6 and 7, respectively. The experimental observations [Figs. 6(d) and 7(d)] indicate the characteristic helical flow patterns in the bend. Figs. 6(a) and 7(a) clearly show that the hydrodynamic results obtained by the angle of repose model showed that it reproduced neither the magnitude and distribution of the velocity in the cross section nor the secondary velocities. The standard Delft3D model [Figs. 6(b) and 7(b)] reproduced the secondary flow patterns, but could not replicate the magnitude and distribution of flow velocity in the cross section mainly due to the inability of the model to predict the erosion in the outer bank. As can be seen in Figs. 6(c) and 7(c), our developed model managed to adequately reproduce the measured velocity magnitude and secondary flow pattern in the cross section.

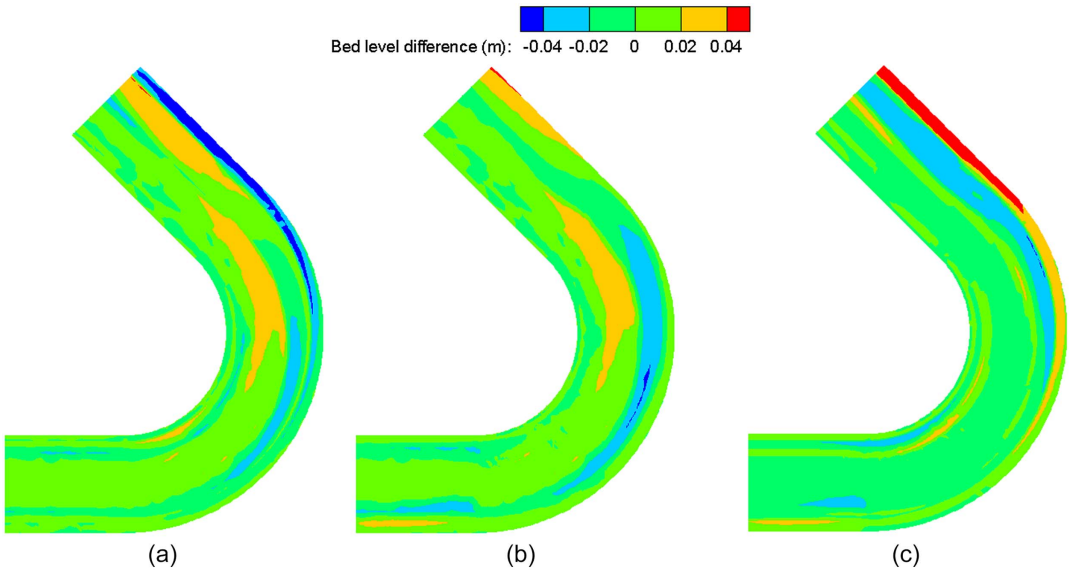


**Fig. 4.** Bed level differences obtained from experimental results relative to (a) standard Delft3D; (b) developed; and (c) angle of repose bank erosion models.

**Table 2.** Comparison of error statistics of bed level computation from each model

| Bank erosion model | MAE (m) | RMSE (m) | Bias error (m) |
|---|---|---|---|
| Developed | 0.010 | 0.014 | 0.002 |
| Standard | 0.013 | 0.016 | 0.011 |
| Angle of repose model | 0.020 | 0.026 | 0.004 |

## Discussion

In general, development of a holistic bank erosion model that works efficiently in all cases is a challenging task. The standard Delft3D model employs a simple bank erosion model in which the erosion flux is transferred to the adjacent dry cell. It may not work effectively once the dry cell gets wet and no more lateral erosion occurs. Thus, it may not be able to simulate the lateral progression of natural rivers. There have been some attempts to properly simulate lateral erosion in the Delft3D code (e.g., Jagers et al. 2011; Spruyt et al. 2011; Canestrelli et al. 2016; Williams et al. 2016). A special version of the bank erosion model has been developed that does simulate large lateral movements of riverbanks (e.g., Spruyt et al. 2011). However, it has not been implemented in standard Delft3D because it only works well in relatively simple, single-thread configurations. Another difficulty in simulating riverbank erosion is updating the new bankline planforms either by regridding or applying immersed boundary techniques (Canestrelli et al. 2016), which require substantial effort to be implemented in the Delft3D code. Thus, the challenge is to develop a bank erosion model that can realistically simulate lateral erosion and can be implemented in the Delft3D source code with manageable effort. Furthermore, the performance of bank erosion models should be evaluated against the entire channel rather than just single cross sections. We attempted to develop a bank erosion method that could be efficiently embedded in the source code of Delft3D with consideration of natural bank erosion processes. Our developed bank erosion code identifies banks and estimates bank erosion fluxes according to Stecca et al. (2017). Its computational cost was compared with that of the standard Delft3D model. Using the same computer, the computational time for different simulations did not change significantly. The developed model's running time was ~18.5 h whereas the running time of the standard Delft3D model was ~18 h.

The performance of our developed model in Delft3D was evaluated against experimental measurements from Jamieson et al. (2013). In addition, it was compared with the Deflt3D standard model and the angle of repose model previously implemented in Delft3D (Williams et al. 2016). We applied the three bank erosion models to the entire experimental channel to ensure that the interaction of the hydrodynamics and morphodynamics in it were considered. The extent and magnitude of the bank scour as well as the hydrodynamics of the channel were examined.

The results show that the estimation of bank erosion flux based only on slope exceedance above a specified angle of repose cannot sufficiently simulate bank erosion processes. They indicate that the angle of repose model leads to unrealistic mass failure in locations where no bank erosion takes place, such as along the inner bank and at side slope transitions (i.e., where the bed and side slope meet and at the top of the side slope). Since this method bases the erosion flux estimation on the exceedance of the bank slope above the repose angle, bank erosion can happen even in the dry areas without any bedload transport (Figs. 3 and 4). This is in agreement with the findings of Stecca et al. (2017) that bank identification and flux estimation are equally crucial. In our developed model, slope exceedance is a required but not sufficient condition for bank erosion to take place.

The angle of repose model better matched the physical (experimental) model bed elevation in the channel thalweg at both 90° and 135° when compared with the standard and developed models. However, as noted previously, it caused excessive bank erosion on both sides of the channel, including along the inner bank, where neither the measurements nor the other two models showed any. It may be that the angle of repose model increased mid-channel bed elevation due to the deposition of the extra sediments transported laterally from the inner bank wall. This emphasizes the fundamental problem with the angle of repose model—it will cause bank erosion with or without fluvial forcing, so the modeler is required to choose an angle of repose that is intermediary, meaning slightly

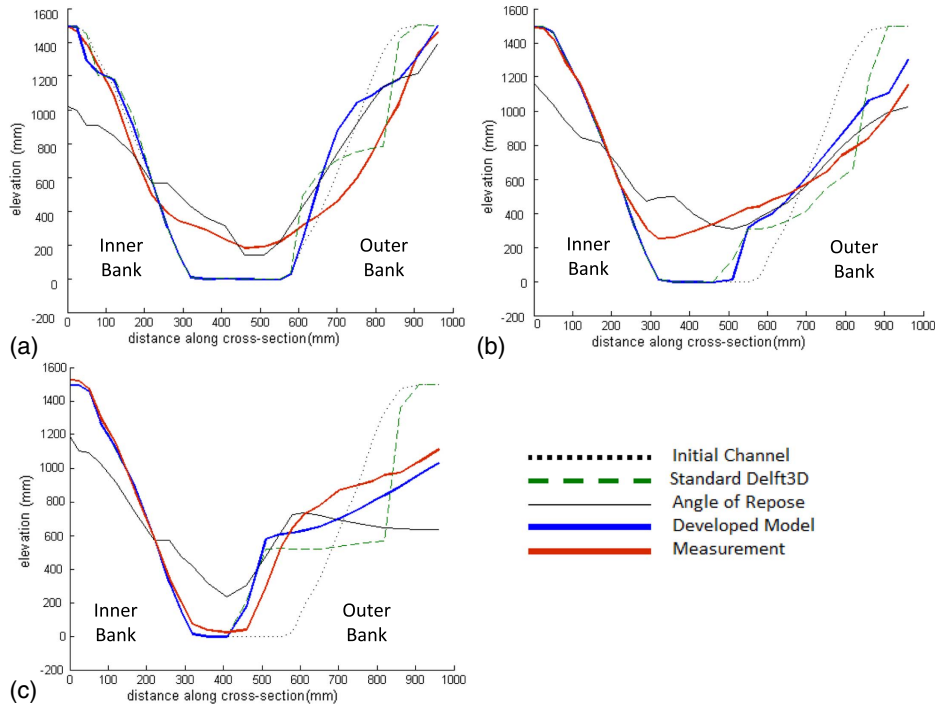


**Fig. 5.** Comparison of bed levels at three cross sections: (a) 90°; (b) 135°; and (c) 1.48 m downstream (d/s) of bend exit. See Fig. 1 for cross section locations.

**Table 3.** Comparison of maximum erosion and deposition

| | Maximum deposition (m) | | | Maximum erosion (m) | | |
|---|---|---|---|---|---|---|
| Experiment/model | 90° cross section | 135° cross section | 1.48 m downstream of bend exit | 90° cross section | 135° cross section | 1.48 m downstream of bend exit |
| Measurements | 0.031 | 0.047 | 0.048 | 0.047 | 0.063 | 0.063 |
| Developed | 0.025 | 0.034 | 0.041 | 0.03 | 0.058 | 0.061 |
| Standard | 0.029 | 0.031 | 0.053 | 0.057 | 0.068 | 0.077 |
| Angle of repose | 0.029 | 0.05 | 0.07 | 0.055 | 0.055 | 0.087 |

greater than the true angle of repose of the sediment but less than what is needed if fluvial erosion is also present.

The results of this study indicate that the standard Delft3D bank erosion module can cause deep scouring near the dry bed rather than in progressive lateral bank erosion. The reasoning for this is as follows. When an erosion flux computed between a wet cell and an adjacent dry cell causes that dry cell to become wet, this cell usually has a small water depth, with limited flow velocity. As a result, the shear stress in it is too small to further erode and no further erosion of neighboring dry cells occurs. Thus, instead of progressive lateral erosion, a steep hole is generated in the cell that experiences higher shear stress. This is not the case for the developed model since the dry cells that become wet can continue to erode due to bank erosion if their slope is above the repose angle and if the toe cell experiences bedload transport.

Overall, the developed bank erosion model yielded better predictions than the other two bank erosion models. Nonetheless, some discrepancies remain between predicted and observed bed morphology. This is to be expected, given the complexity and typical accuracy of sediment transport prediction, particularly in complex flow fields. Importantly, the developed bank erosion model reliably predicted the pattern of erosion and sedimentation.

The results show that not only was bank erosion better predicted in the developed model; secondary flow and streamwise velocity were in better agreement with the measurements compared with those in the angle of repose model and the standard model. This was due to the dependence of both streamwise and transverse velocity on the geometry of the channel, which could change due to bank erosion. On the other hand, velocity distribution and variation in a bend can affect erosion processes and bank scour. For instance, bank erosion in channel bends may cause sharper bends with stronger secondary currents, which in turn may cause different erosion rates. Therefore, an effective bank erosion module is required to not only simulate bank erosion but also accurately predict the hydrodynamics of natural rivers. The results from this study show that the developed model was effective in simulating bank scour along the outer bank and in reproducing the velocity profiles obtained from experimental measurements.

Our developed bank erosion model should provide some insights into bank erosion processes and help improve understanding of the natural migration of meandering rivers. Further studies are needed to examine the performance of the model against field tests where multiple fractions of sediment size may be available and more complex channels with more irregular planform geometry

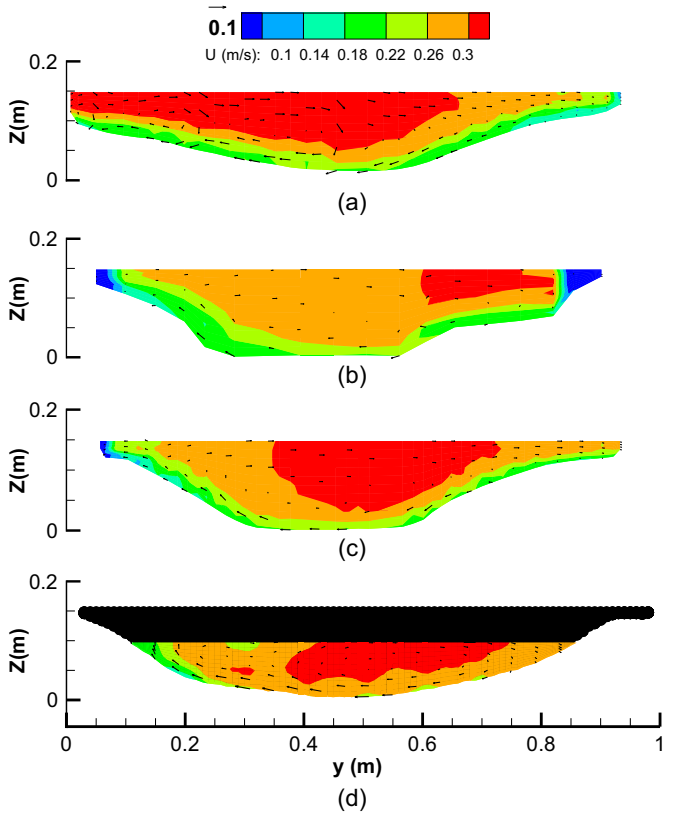


**Fig. 6.** Cross-stream velocity vectors overlaid on streamwise velocity (contour form) at 90° cross section obtained from (a) angle of repose; (b) standard Delft3D; (c) developed bank erosion models; and (d) experimental observations. Black zone shows unmeasured area during ADV measurements.

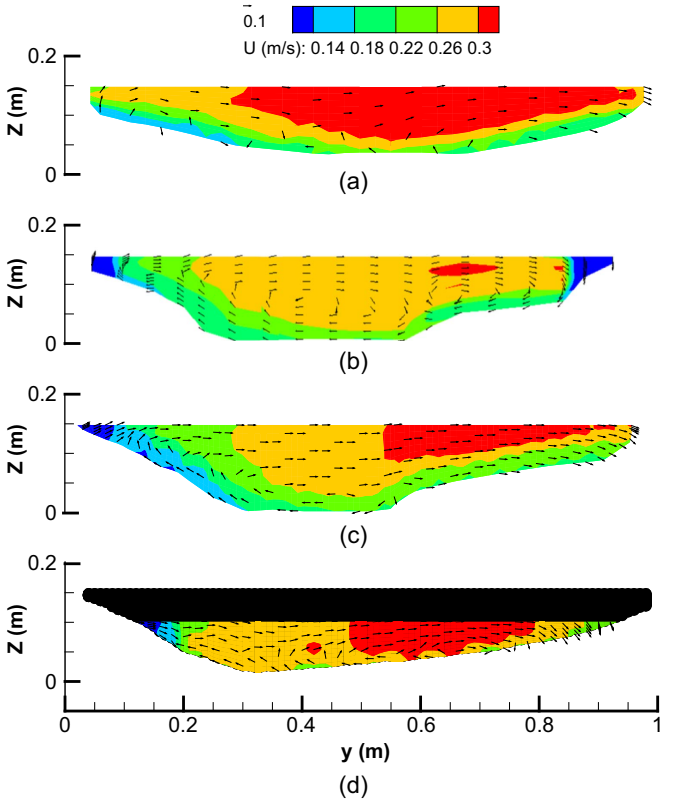


**Fig. 7.** Cross-stream velocity vectors overlaid on streamwise velocity (contour form) at 135° cross section obtained from (a) angle of repose; (b) standard Delft3D; (c) developed bank erosion models; and (d) experimental observations. Black zone shows unmeasured area during the ADV measurements.

may be present. Future studies may also consider other geotechnical and physical processes pertinent to bank erosion, such as pore water pressure in the estimation of bank erosion flux. In addition, the magnitude and direction of bedload transport can be affected by grid resolution. We used relatively fine horizontal and vertical grid resolutions; however, detailed analyses will provide insights into the impact of grid resolution on the simulated morphodynamics of the channel. Moreover, we used the hydrostatic pressure assumption, which may simplify the modeling of secondary flow. However, Parsapour-Moghaddam and Rennie (2017) showed that the 3D hydrostatic Delft3D model can simulate secondary flow in a river bend.

## Conclusion

A new bank erosion model was implemented in Delft3D to better predict progressive lateral bank erosion in natural meandering rivers. Its performance was evaluated against an experimental study of bank erosion in a channel with a sharp bend. The results confirmed that our developed model reasonably reproduces lateral bank erosion as well as the corresponding hydro-morphodynamics in the channel. Moreover, the results were compared with those from the Delft3D standard model and the angle of repose model previously available in the literature. The comparison confirmed the superior performance of the developed model over the other models. The advantages of the developed model are (1) consideration of physical sediment transport compared with the standard Delft3D model; (2) efficient computational cost and straightforward implementation in the Delft3D source code; (3) estimation of bank erosion flux based not just on the exceedance slope but also on bedload transport according to Stecca et al. (2017); and (4) consideration of the complex interaction between bank failure and hydro-morphodynamics in the model evaluation.

## Data Availability Statement

All data, models, or code that support the findings of this study are available from the corresponding author upon reasonable request.

## Acknowledgments

The authors would like to thank The City of Calgary and the Natural Sciences and Engineering Research Council of Canada (Grant CRDJP 524502-18) for funding this project.

## References

Abderrezzak, K. E. K., A. D. Moran, P. Tassi, R. Ata, and J. M. Hervouet. 2016. "Modelling river bank erosion using a 2D depth-averaged numerical model of flow and non-cohesive, non-uniform sediment transport." *Adv. Water Resour.* 93 (May): 75–88. https://doi.org/10.1016/j.advwatres.2015.11.004.

Asahi, K., Y. Shimizu, J. Nelson, and G. Parker. 2013. "Numerical simulation of river meandering with self-evolving banks." *J. Geophys. Res. Earth Surf.* 118 (4): 2208–2229. https://doi.org/10.1002/jgrf.20150.

Bulat, M., P. M. Biron, J. R. Lacey, M. Botrel, C. Hudon, and R. Maranger. 2019. "A three-dimensional numerical model investigation of the impact of submerged macrophytes on flow dynamics in a large fluvial lake." *Freshwater Biol.* 64 (9): 1627–1642. https://doi.org/10.1111/fwb.13359.

Canestrelli, A., A. Spruyt, B. Jagers, R. Slingerland, and M. Borsboom. 2016. "A mass-conservative staggered immersed boundary model for solving the shallow water equations on complex geometries." *Int. J. Numer. Methods Fluids* 81 (3): 151–177. https://doi.org/10.1002/fld.4180.

Chen, D., and J. G. Duan. 2006. "Modeling width adjustment in meandering channels." *J. Hydrol.* 321 (1–4): 59–76. https://doi.org/10.1016/j.jhydrol.2005.07.034.

Constantine, C. R., T. Dunne, and G. J. Hanson. 2009. "Examining the physical meaning of the bank erosion coefficient used in meander migration modeling." *Geomorphology* 106 (3–4): 242–252. https://doi.org/10.1016/j.geomorph.2008.11.002.

Darby, S. E., A. M. Alabyan, and M. J. Van de Wiel. 2002. "Numerical simulation of bank erosion and channel migration in meandering rivers." *Water Resour. Res.* 38 (9): 2–21. https://doi.org/10.1029/2001WR000602.

Deltares. 2020. *Delft3D-FLOW user manual*. Delft, Netherlands: Deltares.

Duan, J. G., and P. Y. Julien. 2005. "Numerical simulation of the inception of channel meandering." *Earth Surf. Processes Landforms* 30 (9): 1093–1110. https://doi.org/10.1002/esp.1264.

Eaton, B. C., M. Church, and R. G. Millar. 2004. "Rational regime model of alluvial channel morphology and response." *Earth Surf. Processes Landforms* 29 (4): 511–529. https://doi.org/10.1002/esp.1062.

Hagemann, L., M. Buchty-Lemke, F. Lehmkuhl, J. Alzer, E. A. Kümmerle, and J. Schwarzbauer. 2018. "Exhaustive screening of long-term pollutants in riverbank sediments of the Wurm River, Germany." *Water Air Soil Pollut.* 229 (6): 197. https://doi.org/10.1007/s11270-018-3843-9.

Hervouet, J.-M. 2007. *Hydrodynamics of free surface flows: Modelling with the finite element method*, 360. Chichester, UK: John Wiley & Sons, Ltd. https://doi.org/10.1002/9780470319628.

Jagers, B., A. Spruyt, and E. Mosselman. 2011. "How to include steep bank retreat in 2D/3D morphological models." In *Proc., AGU Fall Meeting Abstracts*. Washington, DC: American Geophysical Union.

Jamieson, E. C., C. D. Rennie, and R. D. Townsend. 2013. "3D flow and sediment dynamics in a laboratory channel bend with and without stream barbs." *J. Hydraul. Eng.* 139 (2): 154–166. https://doi.org/10.1061/(ASCE)HY.1943-7900.0000655.

Javernick, L., D. M. Hicks, R. Measures, B. Caruso, and J. Brasington. 2016. "Numerical modelling of braided rivers with structure-from-motion-derived terrain models." *River Res. Appl.* 32 (5): 1071–1081. https://doi.org/10.1002/rra.2918.

Kasvi, E., P. Alho, E. Lotsari, Y. Wang, A. Kukko, H. Hyyppä, and J. Hyyppä. 2015. "Two-dimensional and three-dimensional computational models in hydrodynamic and morphodynamic reconstructions of a river bend: Sensitivity and functionality." *Hydrol. Processes* 29 (6): 1604–1629. https://doi.org/10.1002/hyp.10277.

Khosronejad, A., C. D. Rennie, S. A. A. Salehi Neyshabouri, and R. D. Townsend. 2007. "3D numerical modeling of flow and sediment transport in laboratory channel bends." *J. Hydraul. Eng.* 133 (10): 1123–1134. https://doi.org/10.1061/(ASCE)0733-9429(2007)133:10(1123).

Klösch, M., M. Tritthart, and H. Habersack. 2010. "Modeling of near-bank flow velocities during flow events as basis for developing bank erosion equations." In *Proc., River Flow 2010*, 1301–1308. Karlsruhe, Germany: Bundesanstalt für Wasserbau.

Kuntjoro, D. H. 2018. "The movement of the regularly river meanders on constant discharge." *Int. J. Civ. Eng. Technol. (IJCIET)* 9 (6): 619–629.

Lai, Y. G. 2010. "Two-dimensional depth-averaged flow modeling with an unstructured hybrid mesh." *J. Hydraul. Eng.* 136 (1): 12–23. https://doi.org/10.1061/(ASCE)HY.1943-7900.0000134.

Lai, Y. G., R. E. Thomas, Y. Ozeren, A. Simon, B. P. Greimann, and K. Wu. 2015. "Modeling of multilayer cohesive bank erosion with a coupled bank stability and mobile-bed model." *Geomorphology* 243 (May): 116–129. https://doi.org/10.1016/j.geomorph.2014.07.017.

Langendoen, E. J., A. Mendoza, J. D. Abad, P. Tassi, D. Wang, R. Ata, K. El kadi Abderrezzak, and J. M. Hervouet. 2016. "Improved numerical modeling of morphodynamics of rivers with steep banks." *Adv. Water Resour.* 93 (Jun): 4–14. https://doi.org/10.1016/j.advwatres.2015.04.002.

Langendoen, E. J., and A. Simon. 2008. "Modeling the evolution of incised streams. II: Streambank erosion." *J. Hydraul. Eng.* 134 (7): 905–915. https://doi.org/10.1061/(ASCE)0733-9429(2008)134:7(905).

Larsen, E. W., E. H. Girvetz, and A. K. Fremier. 2006. "Assessing the effects of alternative setback channel constraint scenarios employing a river meander migration model." *Environ. Manage.* 37 (6): 880–897. https://doi.org/10.1007/s00267-004-0220-9.

Midgley, T. L., G. A. Fox, and D. M. Heeren. 2012. "Evaluation of the bank stability and toe erosion model (BSTEM) for predicting lateral retreat on composite streambanks." *Geomorphology* 145 (Jun): 107–114. https://doi.org/10.1016/j.geomorph.2011.12.044.

Mosselman, E. 1998. "Morphological modelling of rivers with erodible banks." *Hydrol. Processes* 12 (8): 1357–1370. https://doi.org/10.1002/(SICI)1099-1085(19980630)12:8<1357::AID-HYP619>3.0.CO;2-7.

Nagata, N., T. Hosoda, and Y. Muramoto. 2000. "Numerical analysis of river channel processes with bank erosion." *J. Hydraul. Eng.* 126 (4): 243–252. https://doi.org/10.1061/(ASCE)0733-9429(2000)126:4(243).

Nardi, L., L. Campo, and M. Rinaldi. 2013. "Quantification of riverbank erosion and application in risk analysis." *Nat. Hazards* 69 (1): 869–887. https://doi.org/10.1007/s11069-013-0741-8.

Nicholas, A. P. 2013. "Modelling the continuum of river channel patterns." *Earth Surf. Processes Landforms* 38 (10): 1187–1196. https://doi.org/10.1002/esp.3431.

Olsen, N. R., and S. Stokseth. 1995. "Three-dimensional numerical modelling of water flow in a river with large bed roughness." *J. Hydraul. Res.* 33 (4): 571–581. https://doi.org/10.1080/00221689509498662.

Olsen, N. R. B. 2021. "3D numerical modelling of braided channel formation." *Geomorphology* 375 (Feb): 107528. https://doi.org/10.1016/j.geomorph.2020.107528.

Osman, A. M., and C. R. Thorne. 1988. "Riverbank stability analysis. I: Theory." *J. Hydraul. Eng.* 114 (2): 134–150. https://doi.org/10.1061/(ASCE)0733-9429(1988)114:2(134).

Parker, G., Y. Shimizu, G. V. Wilkerson, E. C. Eke, J. D. Abad, J. W. Lauer, C. Paola, W. E. Dietrich, and V. R. Voller. 2011. "A new framework for modeling the migration of meandering rivers." *Earth Surf. Processes Landforms* 36 (1): 70–86. https://doi.org/10.1002/esp.2113.

Parsapour-Moghaddam, P., C. P. Brennan, C. D. Rennie, C. K. Elvidge, and S. J. Cooke. 2019. "Impacts of channel morphodynamics on fish habitat utilization." *Environ. Manage.* 64 (3): 272–286. https://doi.org/10.1007/s00267-019-01197-0.

Parsapour-Moghaddam, P., and C. D. Rennie. 2017. "Hydrostatic versus nonhydrostatic hydrodynamic modelling of secondary flow in a tortuously meandering river: Application of Delft3D." *River Res. Appl.* 33 (9): 1400–1410. https://doi.org/10.1002/rra.3214.

Parsapour-Moghaddam, P., and C. D. Rennie. 2018. "Calibration of a 3D hydrodynamic meandering river model using fully spatially distributed 3D ADCP velocity data." *J. Hydraul. Eng.* 144 (4): 04018010. https://doi.org/10.1061/(ASCE)HY.1943-7900.0001424.

Piégay, H., S. E. Darby, E. Mosselman, and N. Surian. 2005. "A review of techniques available for delimiting the erodible river corridor: A sustainable approach to managing bank erosion." *River Res. Appl.* 21 (7): 773–789. https://doi.org/10.1002/rra.881.

Rinaldi, M., and S. E. Darby. 2007. "9 Modelling river-bank-erosion processes and mass failure mechanisms: Progress towards fully coupled simulations." *Dev. Earth Surf. Processes* 11 (Feb): 213–239. https://doi.org/10.1016/S0928-2025(07)11126-3.

Rinaldi, M., B. Mengoni, L. Luppi, S. E. Darby, and E. Mosselman. 2008. "Numerical simulation of hydrodynamics and bank erosion in a river bend." *Water Resour. Res.* 44 (9): 1–17. https://doi.org/10.1029/2008WR007008.

Rousseau, Y. Y., M. J. Van de Wiel, and P. M. Biron. 2017. "Simulating bank erosion over an extended natural sinuous river reach using a

universal slope stability algorithm coupled with a morphodynamic model." *Geomorphology* 295 (Aug): 690–704. https://doi.org/10.1016/j.geomorph.2017.08.008.

Shimizu, Y., H. Yamaguchi, and T. Itakura. 1990. "Three-dimensional computation of flow and bed deformation." *J. Hydraul. Eng.* 116 (9): 1090–1108. https://doi.org/10.1061/(ASCE)0733-9429(1990)116:9(1090).

Simon, A., N. Pollen-Bankhead, and R. E. Thomas. 2011. "Development and application of a deterministic bank stability and toe erosion model for stream restoration." In *Stream restoration in dynamic fluvial systems*, 453–474. Washington, DC: American Geophysical Union.

Sinha, S., X. Liu, and M. H. Garcia. 2012. "Three-dimensional hydrodynamic modeling of the Chicago River, Illinois." *Environ. Fluid Mech.* 12 (5): 471–494. https://doi.org/10.1007/s10652-012-9244-5.

Spruyt, A., E. Mosselman, and B. Jagers. 2011. "A new approach to river bank retreat and advance in 2D numerical models of fluvial morphodynamics." In *Proc., 7th IAHS Symp. of River, Coastal and Estuarine Morphodynamics, RCEM 2011*, 1863–1871. Beijng: Tsinghua University Press.

Stecca, G., R. Measures, and D. M. Hicks. 2017. "A framework for the analysis of noncohesive bank erosion algorithms in morphodynamic modeling." *Water Resour. Res.* 53 (8): 6663–6686. https://doi.org/10.1002/2017WR020756.

Theol, S., B. Jagers, J. R. Yangkhurung, F. X. Suryadi, and C. de Fraiture. 2020. "Effect of gate selection on the non-cohesive sedimentation in irrigation schemes." *Water* 12 (10): 2765. https://doi.org/10.3390/w12102765.

Van der Wegen, M., Z. B. Wang, H. H. G. Savenije, and J. A. Roelvink. 2008. "Long-term morphodynamic evolution and energy dissipation in a coastal plain, tidal embayment." *J. Geophys. Res. Earth Surf.* 113 (F3): 1–22. https://doi.org/10.1029/2007JF000898.

Villaret, C., J.-M. Hervouet, R. Kopmann, U. Merkel, and A. G. Davies. 2013. "Morphodynamic modeling using the Telemac finite-element system." *Comput Geosci.* 53 (Apr): 105–113. https://doi.org/10.1016/j.cageo.2011.10.004.

Wallick, J. R., S. T. Lancaster, and J. P. Bolte. 2006. "Determination of bank erodibility for natural and anthropogenic bank materials using a model of lateral migration and observed erosion along the Willamette River, Oregon, USA." *River Res. Appl.* 22 (6): 631–649. https://doi.org/10.1002/rra.925.

Williams, R. D., J. Brasington, M. Hicks, R. Measures, C. D. Rennie, and D. Vericat. 2013. "Hydraulic validation of two-dimensional simulations of braided river flow with spatially continuous aDcp data." *Water Resour. Res.* 49 (9): 5183–5205. https://doi.org/10.1002/wrcr.20391.

Williams, R. D., R. Measures, D. M. Hicks, and J. Brasington. 2016. "Assessment of a numerical model to reproduce event-scale erosion and deposition distributions in a braided river." *Water Resour. Res.* 52 (8): 6621–6642. https://doi.org/10.1002/2015WR018491.

Yan, X., C. D. Rennie, and A. Mohammadian. 2020. "A three-dimensional numerical study of flow characteristics in strongly curved channel bends with different side slopes." *Environ. Fluid Mech.* 20 (6): 1491–1510. https://doi.org/10.1007/s10652-020-09751-9.